ICARUS 108, 186–199 (1994)

The Charon–Pluto Mass Ratio from MKO Astrometry

L. A. YOUNG,[1] C. B. OLKIN,[1] AND J. L. ELLIOT[1,2]

Department of Earth, Atmospheric, and Planetary Sciences, Massachusetts Institute of Technology, Cambridge, Massachusetts 02139-4307
E-mail: lyoung@astron.mit.edu

D. J. THOLEN

Institute for Astronomy, University of Hawaii, Honolulu, Hawaii 96822

AND

M. W. BUIE

Lowell Observatory, Flagstaff, Arizona 86001

Received September 20, 1993; revised November 30, 1993

Using the UH 2.2-m telescope, we obtained CCD images of Pluto as it passed through a single field of 10 stars during 6 nights of Charon's 6.4-day orbital period. From these data, Charon's orbital semimajor axis is found to be 19,460 ± 58 km, which is consistent with the recent measurement by Null *et al.* (1993, *Astron. J.* 105, 2319–2335) of 19,405 ± 86 km. Our semimajor axis implies a system mass of (14.32 ± 0.13) × 10^{24} g. From the motions of Pluto and Charon around their barycenter, we find that the ratio of Charon's mass to Pluto's is 0.1566 ± 0.0035, indicating that the bodies both have densities near 2 g cm^{-3}. Our ratio is nearly twice that of Null *et al.*, who find a ratio of 0.0837 ± 0.0147. Possible reasons for the large discrepancy are discussed.

1. INTRODUCTION

From the densities of Pluto and Charon, one can derive the rock–ice fractions of these bodies. These reflect the cosmochemical abundances at the time of their formation and their evolution. Also, the relative densities of Pluto and Charon can constrain scenarios for the formation of the Pluto–Charon binary (McKinnon 1989). The masses control the dynamics of the system, including the time scales for tidal lock and the escape rates of volatiles. Furthermore, the relative masses are necessary for predictions of stellar occultations. For example, a change in Charon's assumed density from 1 to 2 g cm^{-3} can move the predicted position of Pluto's shadow by more than half its width.

The densities are functions of the radii, the system mass, and the ratio of the two masses. Radii of Pluto and Charon have been measured from the mutual events and from stellar occultations. One stellar occultation has been observed for each body. Elliot and Young (1991) reanalyzed a 1980 occultation by Charon (Walker 1980) and found a 3σ lower limit on Charon's radius of 601.5 km. Millis *et al.* (1993) performed a joint solution of all observations of the 1988 occultation by Pluto, using the occultation light curve model for small bodies developed by Elliot and Young (1992). They found that Pluto's radius is 1195 ± 5 km if the lower atmosphere is clear, and smaller than 1180 ± 5 km if there is a haze layer. Tholen and Buie (1990, hereafter TB90) found radii of Pluto and Charon of 1151 ± 6 km and 593 ± 13 km from their analysis of the mutual-event season. Larger radii (1190 ± 20 km and 642 ± 11 km) were found by Young (1992), also from the mutual-event season. He noted the extremely strong correlation between radii determined from the mutual events and the amount of limb darkening assumed. The scale of the system for the mutual events is set by a, the semimajor axis of Charon's orbit around Pluto. TB90 used a = 19,640 km (Beletic *et al.* 1989). More recent observations suggest a smaller semimajor axis (Null *et al.* 1993, hereafter NOS93), which decreases the mutual-event values for Pluto's radius by 14 km, and for Charon's radius by 7 km.

Pluto and Charon orbit around the system barycenter with semimajor axes a_p and a_c. The ratio of their masses ($q = M_c/M_p$) equals the ratio of these semimajor axes, and the sum of their masses is proportional to a^3. Thus,

[1] Visiting observer, 2.2-m telescope at Mauna Kea Observatory, Institute for Astronomy, University of Hawaii.

[2] Also Department of Physics, Massachusetts Institute of Technology, and Lowell Observatory.

Presented at the conference "Pluto and Charon," Flagstaff, AZ, July 1993.

0019-1035/94 $6.00

the individual masses can be found by measuring $a = a_p + a_c$ and $q = a_p/a_c$. NOS93 measured a and q by observing the motion of Pluto and Charon on CCD images obtained with the Hubble Space Telescope (HST). These observations suffered from three major limitations: (i) the reimaging optics introduced large field distortions; (ii) only one star was present in the same field as Pluto, so Pluto itself had to provide the relative orientations of the observations; and (iii) only half of the Charon orbital period was observed.

Our approach avoids these limitations and provides an independent measurement of the masses. The large field of view available on ground-based telescopes afforded us the following advantages: (i) the telescope could be used in direct imaging mode, where the optics introduce negligible field distortion; (ii) 10 field stars were observed in our field, allowing for precise registration of exposures; and (iii) Pluto and Charon remained within this set of 10 field stars on six successive nights of observation, or 78% of the orbit. Although the images of Pluto and Charon are usually blended in ground-based observations, the image can be successfully modeled as the sum of two point sources. For example, Jones *et al.* (1988) measured the separation of Pluto and Charon with a standard deviation of 0.004 arcsec. The data on our best night reach a similar precision.

This paper is divided into seven sections. We describe the observations in Section 2. Next, we present our analysis, including (a) the method for finding centers, (b) the use of the field stars to register the exposures, and (c) the model we used to find the orbits, the mass ratio, and the plate constants. In Section 4, we apply this model and perform various sensitivity tests. We place bounds on systematic errors in Section 5. We discuss our results in Section 6, and summarize our conclusions in Section 7.

2. OBSERVATIONS

We obtained images of Pluto, Charon, and field stars from 1992 February 26 to March 2 with the University of Hawaii 2.2-m telescope at Mauna Kea. The telescope is an f/10 Ritchey–Chrétien, which we used in direct imaging mode for maximum transmission and minimum field distortion. The detector, a 1024 × 1024 Tektronics CCD, had a nominal image scale of 0.22 arcsec per pixel for a field of view of 225 arcsec on a side. Images were taken in B, V, R, and I. Only the B exposures are analyzed in this paper.

Our observing run consisted of the 2 hours before each morning twilight on 1992 February 25 to March 2. High winds precluded observations on February 25, and delayed the start of observations on February 26. Table I

TABLE I
Observation Log

Date	Time (UT)	Object	FWHM (")	Predicted Separation (")	Exposures Converged/Observed	Pluto center of light[a] Δx (km)	Pluto center of light[a] Δy (km)	Charon center of light[a] Δx (km)	Charon center of light[a] Δy (km)
1992 Feb 26	15:29 – 16:03	Pluto/Charon	1.24	0.75	15/18	58	80	51	4
1992 Feb 27	14:05 – 14:33	Pluto/Charon	1.20	0.88	16/16	–90	52	51	45
	14:37 – 15:42	1981 Midas	–	–	32/32	–	–	–	–
	15:47 – 15:50	Pluto/Charon	1.21	0.86	4/4	–86	49	47	46
1992 Feb 28	13:55 – 14:43	1981 Midas	–	–	28/28	–	–	–	–
	14:48 – 15:17	Pluto/Charon	1.23	0.30	4/16	–7	38	–49	18
1992 Feb 29	13:52 – 14:17	Pluto/Charon	0.88	0.59	4/14	–8	53	–46	7
	14:24 – 15:16	1981 Midas	–	–	21/21	–	–	–	–
	15:20 – 15:25	Pluto/Charon	1.02	0.63	2/4	–7	53	–42	8
1992 Mar 1	13:58 – 14:10	Pluto/Charon	0.98	0.91	8/8	–39	58	3	24
	14:20 – 15:05	1981 Midas	–	–	28/28	–	–	–	–
	15:11 – 15:29	Pluto/Charon	0.91	0.91	12/12	–43	57	3	24
1992 Mar 2	13:51 – 14:27	Pluto/Charon	0.99	0.46	19/20	–1	24	–20	–6
	14:40 – 15:23	1981 Midas	–	–	28/28	–	–	–	–

[a] The offset from the center of each body to the center of light, determined from the albedo map of Buie *et al.* (1992). The $+x$ direction is toward the receding limb and the $+y$ direction is toward Pluto's or Charon's rotational north pole.

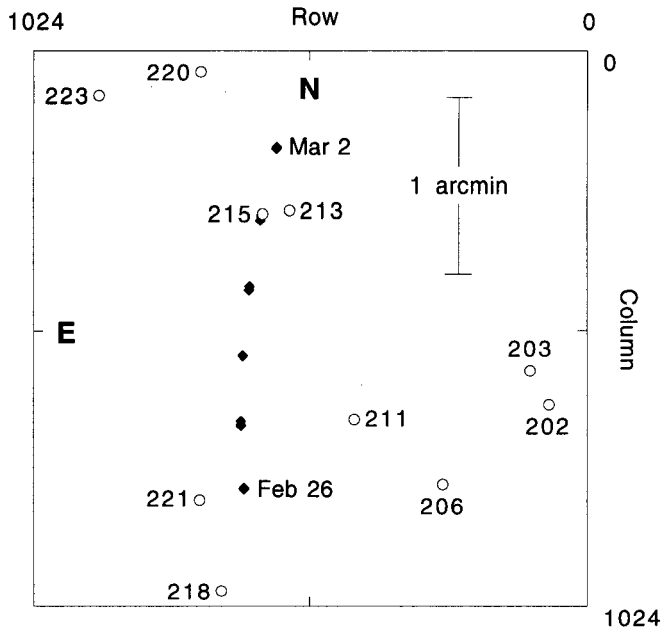

FIG. 1. Pluto and field stars for 1992 February 26–March 2. The open circles and 3-digit IDs mark the mean positions of the field stars brighter than ~18 mag. The black diamonds mark the location of Pluto on each of the six nights of observation. On February 27, February 29, and March 1, the distance Pluto covered in a single night is indicated by double diamonds. The dates of the first and last nights of observations are indicated. The image scale was 0.22 arcsec/pixel.

shows a log of our observations. We increased our data rate by taking multiple exposures before reading out the CCD, moving the telescope 10 arcsec south between exposures. The telescope tracked at the Pluto rate. We typically took four exposures of 60 sec each, with approximately 10 sec between exposures. Asteroid 1981 Midas was also observed to establish the plate constants from its motion across the field. This object was chosen for three reasons: (i) the motion was known to within a few parts in 10^6 (Marsden 1989); (ii) Midas crossed the field of view in less than an hour, which made it feasible to observe Midas while still getting good coverage on Pluto; and (iii) Midas was 6°–15° from Pluto during the observing run. Four exposures of the Midas field were taken before reading out the CCD. The telescope tracked at the sidereal rate during observations of Midas and was not offset between exposures.

Because Pluto passed through a stationary point in right ascension during the observing run, the motion was primarily in declination and spanned only 138 arcsec. Pluto could therefore be captured in a single field during the 6-day observing run (Fig. 1). Two occultation candidate searches report approximate positions for stars near Pluto's path. One search was conducted at the Smithsonian Astrophysical Observatory with observations from Lick Observatory (Mink *et al.* 1991), using the Perth 70 catalog for reduction to a standard reference frame (Høg and von der Heide 1976). A deeper search was conducted at the Massachusetts Institute of Technology with observations from MIT's Wallace Astrophysical Observatory in Westford, MA (Dunham *et al.* 1991), using the Lick–SAO positions as a secondary astrometric network. The IDs used in this paper were assigned by the MIT occultation search team. We performed photometry of selected field stars in 1992 June at Lowell Observatory in Flatstaff, AZ. These observations are summarized in Table II.

The frames were calibrated in the standard manner, with bias subtraction, dark subtraction, and flat fielding. Bias levels were found for each frame from an overscan region. The dark current, determined from a 3600-sec dark exposure, was less than 1 ADU for the Pluto exposures. The flat for each night was the median of 3 or 4 dome flats. These flats appeared adequate; out-of-focus dust grains visible on the flats were undetectable in the flattened images.

3. ANALYSIS

A. Centers of Pluto, Charon, Midas, and Field Stars

Least-squares fitting of point-spread functions (PSFs) is an effective method for analyzing crowded fields. The stars on the field define the PSF, which is then fit to all objects of interest to find centers and brightnesses. In our analysis, most of the steps used the IRAF implementation of DAOPHOT (Stetson 1987). Ordinarily, DAOPHOT determines the background for a star from a sky annulus. Because of the multiple exposures, every star in the Pluto field has one or two stars 10 arcsec away that could inflate the estimate of the local background. To avoid this, we removed the background by fitting a second-order polynomial through the local background (determined by the median of the surrounding 100 × 100 box). Because DAOPHOT assigns weights based on Poisson statistics, a constant was added back to the image to restore the mean background level. This constant was used as the background for that frame in subsequent analyses.

The PSFs were constructed from field stars with the PSF routine of DAOPHOT. For the Pluto–Charon frames, the PSFs did not include star 206 (its profile was noticeably narrower than those of the other field stars), star 211 (it had two faint stars 3 arcsec away), or for the night of March 1, star 215 (it was too close to Pluto and Charon). Because the Pluto field was offset between exposures, star 218 never appears on the first exposure, and star 220 never appears on the fourth. For the Midas frames, the PSF simply included the 5 to 10 brightest field stars.

We used the NSTAR routine of DAOPHOT to fit for the centers and brightnesses of objects on the Pluto expo-

TABLE II
Astrometry and Photometry of Field Stars

MIT occultation search (Dunham *et al.* 1991)				Lick-SAO occultation search (Mink *et al.* 1991)				Lowell photometry (This work)		
ID	α (J2000)	δ (J2000)	CCD mag[a]	ID	α (J2000)	δ (J2000)	V[b]	B	V	R
202	15 37 28.78	-4 01 19.4	13.3	1497	15 37 28.798	-4 01 19.40	14.3	14.60	13.69	13.20
203	15 37 29.30	-4 01 05.6	13.1	1499	15 37 29.311	-4 01 05.26	14.1	14.27	13.46	13.03
206	15 37 31.63	-4 01 51.7	12.4	1502	15 37 31.642	-4 01 51.35	13.7	14.26	12.93	12.22
211	15 37 34.02	-4 01 25.6	15.1	1506	15 37 34.029	-4 01 25.67	15.1	16.54	15.52	15.01
213	15 37 35.80	-4 00 01.3	16.6							
215	15 37 36.53	-4 00 02.8	15.5	1510	15 37 36.540	-4 00 02.72	15.2	16.64	15.79	15.30
218	15 37 37.62	-4 02 35.5	15.9	1511	15 37 37.632	-4 02 35.50	15.3			
220	15 37 38.23	-3 59 06.5	15.0	1514	15 37 38.222	-3 59 06.34	15.2			
221	15 37 38.22	-4 01 57.9	17.5							
223	15 37 40.98	-3 59 16.3	17.5							

[a] CCD with no filter; approximately R magnitude.
[b] Approximate magnitude.

sures. As with all PSF-fitting routines, NSTAR attempts to minimize the weighted sum of the square of the residual image. Pluto and Charon were fit simultaneously, and star 215 was included in the simultaneous fit for the night of March 1. Figure 2 shows the results of a fit to a typical blended Pluto–Charon image. NSTAR was originally designed for crowded-field photometry of stars; if the signal-to-noise ratio of the dimmer of two objects in a simultaneous fit is too low, the routine interprets this as an erroneous detection of the second object. The number of exposures for which the fit successfully converged is listed in Table I. As NSTAR does not report the errors in the centers it finds, errors were assigned to the centers on the basis of the width of the best-fitting Gaussian and the errors in the signal (King 1983) as

$$\frac{\sigma_x}{w} = k\frac{\sigma_s}{s}, \tag{1}$$

where σ_x is the error in the position, w is the width of a Gaussian, σ_s is the error in the peak signal, and s is the peak signal. The coefficient k depends on the shape of the PSF; we used $\sqrt{2}$, which is appropriate for a Gaussian PSF.

Because of the large albedo variation over Pluto's surface, the fitted centers of Pluto and Charon were the center of light, not the center of disk. From the maximum-entropy solution to the mutual event and rotational lightcurves (Buie *et al.* 1992), we calculated the predicted distance between the center of light and the center of disk for each exposure. Table I includes the average offsets in x (toward the receding limb) and y (toward the rotational north pole). These were converted to offsets in row and column from a preliminary solution for the orbit and plate constants, and subtracted from the center-of-light positions. A listing of object centroids will be available on request from the authors.

Since Midas moved 7 to 12 pixels during an exposure, the PSF was convolved with Midas' motion to model the elongated image. The "Midas-spread function" was fit to the Midas images and the unconvolved PSF to the field stars. Because DAOPHOT does not handle this case easily, we used our own least-squares package.

B. Registration of Exposures

The star centers defined the astrometric relationship between the different exposures. A set of coefficients (a_{ij}, b_{ij}) linearly converted the rows and columns (r and c) for a given exposure to the transformed rows and columns (r_{trans} and c_{trans}) of a reference frame:

$$\begin{aligned} r_{\text{trans}} &= a_{00} + a_{10}r + a_{01}c \\ c_{\text{trans}} &= b_{00} + b_{10}r + b_{01}c. \end{aligned} \tag{2}$$

We built up the reference frame by minimizing the weighted scatter of each star's transformed positions around its mean transformed position. One exposure was chosen to define the absolute scale of the reference frame; for this exposure, $r = r_{\text{trans}}$ and $c = c_{\text{trans}}$. The Pluto and

Charon positions are transformed to the reference frame as well.

The Midas frames for each night were registered in a similar manner. Since the Midas observations were used to determine the image scale and orientation, the centers of the field stars and Midas were corrected for differential aberration and refraction before the exposures were registered. The differential changes in position were cast as linear equations in row and column, using the linear terms from Green (1985, Eqs. (13.24) and (13.32)). Correcting for differential refraction and aberration decreased the image scale by 3 parts in 10^4 and had no significant effect on the orientation.

C. Model Rows and Columns

The first step in calculating the rows and columns of Pluto and Charon is finding the apparent orbit of Charon around Pluto. TB90 found that the eccentricity of Charon's orbit around Pluto was 0.00020 ± 0.00021, unless the longitude of perihelion happened to be along the line of sight, in which case it could be as high as 0.01. The eccentricity is assumed to be zero for this analysis. The remaining orbital elements, shown in Fig. 3, are the inclination (i), the longitude of the ascending node (Ω), the argument of latitude (u, identical to TB90's "mean anomaly, measured from the ascending node"), and the semi-major axis of Charon's orbit around Pluto (a, not shown).

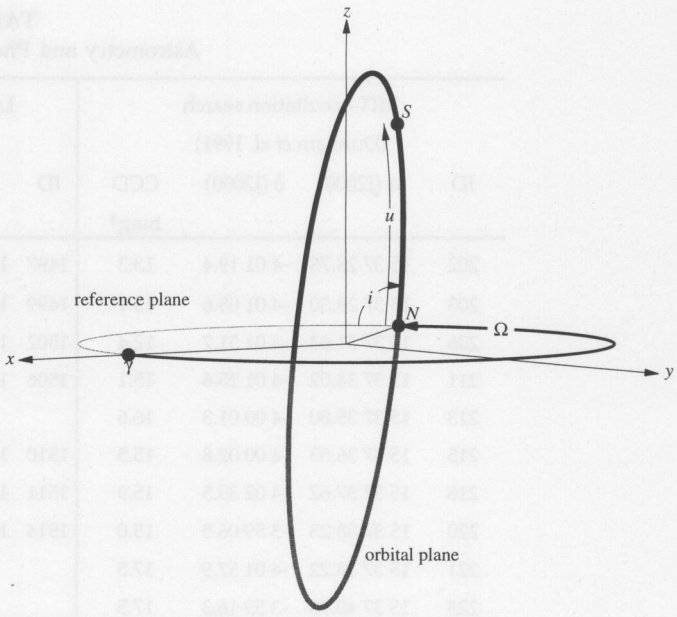

FIG. 3. Orbital elements. The apparent ellipse depicted was generated using Charon's orbital elements. The line-of-sight vector is perpendicular to the paper, so this figure depicts Charon's orbit as seen from Earth. The angles indicated are the longitude of the ascending node (Ω), the inclination (i), and the argument of latitude (u). The dots indicate the position of the satellite (S), the ascending node (N), and the origin of the longitude (γ).

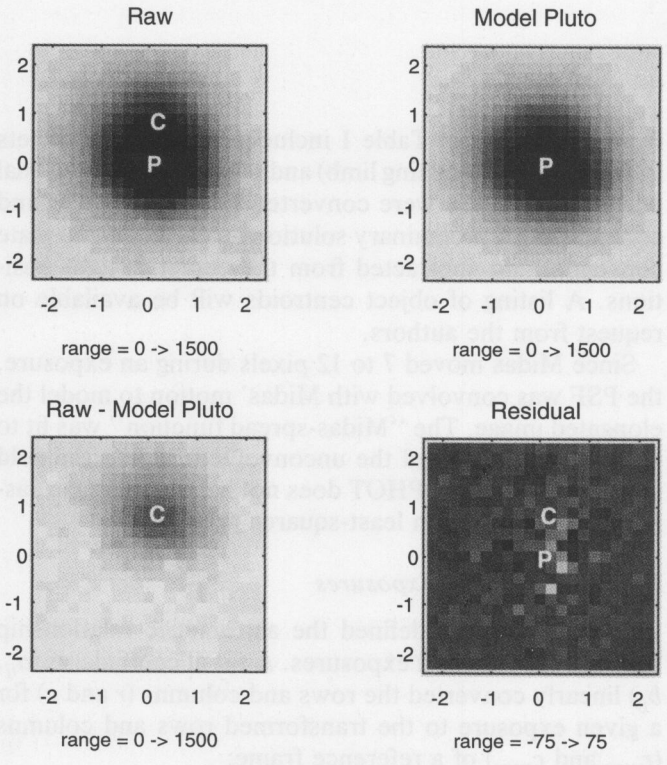

FIG. 2. Typical Pluto/Charon image. The upper left shows the image after background subtraction. The letters "P" and "C" mark the positions of Pluto and Charon. A simultaneous fit was performed for the centers and brightnesses of Pluto and Charon. The model Pluto, in the upper right, is a scaled and shifted model PSF. The lower left shows the image with the model Pluto subtracted. The remaining image, which should be just Charon, has the same shape as the model Pluto. The lower right shows the residual when both the model Pluto and the model Charon are subtracted. The scale is increased by a factor of 10, and no systematic residual is apparent. The axes are marked in arcsec. North is up and east is to the left.

All calculations involving the right ascension (α) and declination (δ) are performed in tangent-plane ("standard") coordinates (ξ and η). These are obtained by gnomonic projection, the projection of the celestial sphere onto a plane tangent at a given right ascension and declination (α_0, δ_0) (Green 1985, Eq. (13.12)):

$$\xi = \frac{\cos\delta \sin(\alpha - \alpha_0)}{\sin\delta_0 \sin\delta + \cos\delta_0 \cos\delta \cos(\alpha - \alpha_0)}$$
$$\eta = \frac{\cos\delta_0 \sin\delta - \sin\delta_0 \cos\delta \cos(\alpha - \alpha_0)}{\sin\delta_0 \sin\delta + \cos\delta_0 \cos\delta \cos(\alpha - \alpha_0)}. \quad (3)$$

From the orbital elements and the position of the barycenter (α_b and δ_b), the difference in the standard coordinates of Pluto (ξ_p, η_p) and Charon (ξ_c, η_c) is adequately defined by

$$\begin{bmatrix} \xi_c - \xi_p \\ \eta_c - \eta_p \end{bmatrix} = \frac{a}{\Delta} \begin{bmatrix} -\sin(\alpha_b - \Omega) & \cos(\alpha_b - \Omega)\cos i \\ -\cos(\alpha_b - \Omega)\sin \delta_b & -\sin(\alpha_b - \Omega)\sin \delta_b \cos i \\ & + \cos \delta_b \sin i \end{bmatrix} \cdot \begin{bmatrix} \cos u \\ \sin u \end{bmatrix} \quad (4)$$

where Δ is the Earth–Pluto distance.

The rotational phase (p) and (under the assumption of a circular orbit) the argument of latitude increase at a constant rate, starting from initial values p_0 and u_0 defined at an initial Julian date, JD_0. If JD is the time of observation, then

$$\frac{u - u_0}{360^\circ} = p - p_0 = \frac{JD - (\Delta/c) - JD_0}{P}, \quad (5)$$

where c is the speed of light (173 AU/day) and P is the period, for which we adopt 6.387246 ± 0.000011 days from TB90. To compare results with TB90, we use their epoch, JD2446600.5. At 1992 Mar 1 9 : 53 : 27 UT, an integral number of orbits had occurred since JD_0, so at that time $u = u_0$ and $p = p_0 = 0.46111$. The phase is calculated using the definition of Binzel *et al.* (1985), with the substitution of TB90's value for the period.

The standard coordinates relative to the barycenter depend on the mass ratio, q:

$$\begin{bmatrix} \xi_p \\ \eta_p \end{bmatrix} = \begin{bmatrix} \xi_b \\ \eta_b \end{bmatrix} - \frac{q}{1+q} \begin{bmatrix} \xi_c - \xi_p \\ \eta_c - \eta_p \end{bmatrix}$$
$$\begin{bmatrix} \xi_c \\ \eta_c \end{bmatrix} = \begin{bmatrix} \xi_b \\ \eta_b \end{bmatrix} + \frac{1}{1+q} \begin{bmatrix} \xi_c - \xi_p \\ \eta_c - \eta_p \end{bmatrix}. \quad (6)$$

We generated a light-time corrected geocentric J2000 ephemeris of the barycenter at 10-min intervals from JPL's DE202 ephemeris (Standish 1987) using the SPICELIB library provided by the NAIF group at JPL (Acton 1990). These were linearly interpolated to the times of observations, and converted to topocentric α and δ. We then calculated ξ_b and η_b from Eq. (3), choosing a tangent point whose J2000 position was near the center of the CCD: $\alpha_0 = 15^h37^m35^s$, $\delta_0 = -4°00'55''$.

The standard coordinates were transformed linearly to the row and column of the reference frame using the plate constants m_{11}, m_{12}, m_{21}, and m_{22}:

$$\begin{bmatrix} r_{trans} \\ c_{trans} \end{bmatrix} = \begin{bmatrix} r_0 \\ c_0 \end{bmatrix} + \begin{bmatrix} m_{11} & m_{12} \\ m_{21} & m_{22} \end{bmatrix}^{-1} \times \begin{bmatrix} \xi \\ \eta \end{bmatrix}. \quad (7)$$

The free parameters (q, a, i, Ω, u_0, m_{11}, m_{12}, m_{21}, m_{22}, r_0, c_0) were adjusted to minimize (in a least-squares sense) the difference between the model and the observed rows and columns.

4. RESULTS

In this section, we apply the model of Section 3 to the centers of Pluto and Charon. In the first battery of fits (Table IIIa), we do not constrain any parameters. We first apply the model to all converged Pluto and Charon centers (Fit #1). The night of February 28 is a poor fit to the model for the following reasons: (i) we will see in Section 5 that the position of Charon is particularly sensitive to the shape of the constructed PSF on this night; (ii) the FWHM is large while the separation is small; (iii) fits to only 4 out of 16 exposures converged; and (iv) the errors assigned to the Charon centers on February 28 were seven times larger than on the other nights. When the fitted data do not include February 28 (Fit #2), the mean residuals are much lower, but the mass ratio changes by only a third of its formal error. For the remainder of the paper, we exclude February 28 from the analysis. Fits #3–6 include just the first, second, third, or fourth exposure on each frame. Since the four exposures were offset from one another by 10 arcsec, fitting one exposure at a time tests if the results are strongly dependent on the locations of the images. The average scatter of the parameters for Fits #3–6 is close to twice the formal error of Fit #2, as expected because only one quarter of the data was used. The scatter for q is somewhat higher, at 3.2 times the formal error of Fit #2. We fit for the Pluto positions alone, in Fit #7. In this fit, we need to fix a, because we are effectively fitting for Pluto's orbital semimajor axis, $a_p = aq(1 + q)^{-1}$. The amplitude of the Pluto wobble is consistent with Fit #2, but the other elements are not as well determined.

In the second battery of fits (Table IIIb), we used all the centers except those from the night of February 28, and fixed various parameters. The independently determined values and errors for the fixed parameters are parenthesized in Table IIIb. Fit #8 fixes the shape of the orbit by fixing i, u_0, and Ω at the TB90 orbital elements, precessed to the J2000 equinox. TB90's formal errors in u_0 and Ω are smaller than those from the imaging observations of this work (Fit #2) and NOS93. This is true even if we consider the additional 0.20° error in u_0 that arises from propagating the error in the period forward from JD_0. The mutual events are most sensitive to the elements best measured at minimum separation: the timing of the orbit (controlled mainly by u_0) and the width of the apparent ellipse (controlled mainly by Ω). In contrast, imaging is more sensitive to those elements measured at elongation: the semimajor axis of the orbit (controlled entirely

TABLE IIIa
Sensitivity to Choice of Data

	Fit #1 All data	Fit #2 No Feb. 28	Fit #3 No Feb. 28 First Exposures	Fit #4 No Feb. 28 Second Exposures	Fit #5 No Feb. 28 Third Exposures	Fit #6 No Feb. 28 Fourth Exposures	Fit #7 No Feb. 28 Pluto alone
q	0.1554 ± 0.0035	0.1565 ± 0.0035	0.1425 ± 0.0045	0.1581 ± 0.0055	0.1702 ± 0.0047	0.1555 ± 0.0048	0.1644 ± 0.0093
a (km)	19489 ± 64	19484 ± 64	19621 ± 91	19520 ± 103	19539 ± 83	19382 ± 74	(19484)
i (deg)	95.17 ± 0.27	95.15 ± 0.27	95.12 ± 0.38	94.52 ± 0.43	95.16 ± 0.35	95.74 ± 0.34	87.80 ± 3.10
Ω (deg)	222.52 ± 0.86	222.46 ± 0.87	222.91 ± 1.01	222.09 ± 1.44	222.08 ± 1.17	223.28 ± 1.27	225.52 ± 8.99
u_0 (deg)	260.48 ± 0.64	260.37 ± 0.64	260.62 ± 0.75	259.71 ± 1.07	260.29 ± 0.91	260.41 ± 0.91	269.07 ± 7.42
m_{11} (mas/pix)	218.071 ± 0.157	218.086 ± 0.158	218.594 ± 0.196	217.899 ± 0.258	217.594 ± 0.207	217.806 ± 0.222	218.609 ± 1.079
m_{12} (mas/pix)	–0.601 ± 0.015	–0.602 ± 0.015	–0.642 ± 0.019	–0.576 ± 0.025	–0.554 ± 0.021	–0.599 ± 0.022	–0.722 ± 0.104
m_{21} (mas/pix)	–0.410 ± 0.120	–0.347 ± 0.122	–0.053 ± 0.150	–0.386 ± 0.200	–0.333 ± 0.171	–0.816 ± 0.180	0.697 ± 0.908
m_{22} (mas/pix)	–218.477 ± 0.016	–218.485 ± 0.016	–218.485 ± 0.021	–218.445 ± 0.027	–218.508 ± 0.024	–218.471 ± 0.027	–218.588 ± 0.088
r_0 (pix)	487.846 ± 0.089	487.854 ± 0.090	488.105 ± 0.111	487.745 ± 0.148	487.585 ± 0.119	487.723 ± 0.128	488.156 ± 0.614
c_0 (pix)	506.945 ± 0.069	506.911 ± 0.069	506.750 ± 0.085	506.921 ± 0.115	506.873 ± 0.098	507.193 ± 0.103	506.317 ± 0.517
σ_p (mas)	11	11	9	8	7	8	9
σ_c (mas)	56	22	20	20	23	19	–

Note. All parameters are unconstrained. Parenthesized values were not fit.

TABLE IIIb
Sensitivity to Fixing Parameters

	Fit #8 orbital elements from TB90	Fit #9[a] Ω and u_0 from TB90	Fit #10 plate constants from Midas	Fit #11 plate constants fromMIT astrom.	Fit #12 q from NOS93
q	0.1553 ± 0.0049	0.1566 ± 0.0035	0.1597 ± 0.0013	0.1736 ± 0.0047	(0.0837 ± 0.0147)[b]
a (km)	19542 ± 82	19460 ± 58	19464 ± 64	19392 ± 215	19428 ± 105
i (deg)	(99.10 ± 1.00)	95.00 ± 0.24	95.09 ± 0.27	91.78 ± 0.91	95.38 ± 0.45
Ω (deg)	(223.01 ± 0.03)	(223.01 ± 0.03)	223.41 ± 0.81	224.19 ± 2.77	222.46 ± 1.41
u_0 (deg)	(259.76 ± 0.08)[c]	(259.76 ± 0.08)[c]	259.63 ± 0.61	258.79 ± 2.06	260.99 ± 1.04
m_{11} (mas/pix)	218.196 ± 0.203	218.132 ± 0.144	(218.478 ± 0.061)	(219.164 ± 0.127)	218.688 ± 0.233
m_{12} (mas/pix)	–0.598 ± 0.020	–0.606 ± 0.014	(–0.621 ± 0.064)	(–0.985 ± 0.107)	–0.673 ± 0.023
m_{21} (mas/pix)	–0.395 ± 0.156	–0.390 ± 0.112	(–0.619 ± 0.260)	(–0.773 ± 0.167)	–1.100 ± 0.174
m_{22} (mas/pix)	–218.477 ± 0.022	–218.481 ± 0.016	(–218.471 ± 0.120)	(–218.505 ± 0.141)	–218.213 ± 0.017
r_0 (pix)	487.909 ± 0.115	487.880 ± 0.082	488.070 ± 0.005	488.572 ± 0.016	488.200 ± 0.132
c_0 (pix)	506.939 ± 0.089	506.935 ± 0.063	507.062 ± 0.004	507.140 ± 0.013	507.350 ± 0.098
σ_p (mas)	11	11	12	45	18
σ_c (mas)	44	24	27	74	27

Note. All data were used except February 28.

[a] Adopted solution.

[b] Parenthesized values were not fit. The parenthesized errors, taken from the same sources as the corresponding values, do not affect the fit in any way and are included for comparison only.

[c] This is the error for u_0 at JD_0. Due to the 5.7-yr span between JD_0 and the observations, the effective error in u_0 increases to 0.22°.

by a) and the orientation of the apparent ellipse (controlled mainly by i). Fit #9 uses u_0 and Ω from TB90. Because Fit #9 is consistent with the unconstrained fit (Fit #2), with fewer degrees of freedom, we adopt Fit #9 as our solution.

We can determine the plate constants from the motion of Pluto, the motion of 1981 Midas, and the locations of the field stars. Midas moved in essentially a straight line across the field, providing the image scale and orientation. These are converted to plate constants (m_{11}, m_{12}, m_{21}, m_{22}) for Fit #10, and adjusted for the differential refraction and aberration appropriate for the reference frame. For Fit #11, we fixed the plate constants at those determined by an unweighted fit of the mean star positions to the positions found by the MIT occultation search.

Fits #1–11 all give mass ratios much larger than the value of 0.0837 ± 0.0147 found by NOS93. Fit #12 demonstrates what happens when we force a small value of q on our observations. The rms Pluto residuals are 40% larger than those for the adopted solution. Pluto's barycentric orbit and residuals for the adopted solution and for the low-q solution are shown in Fig. 4. For the adopted solution, the nightly means in the residuals of $\eta_p - \eta_b$ are scattered around zero. In contrast, the nightly mean residuals for the low-q solution are as large as 26 milliarcsec, and the residuals are quantitatively sinusoidal. Clearly, we did not achieve a good fit when we fixed the mass ratio at such a low value.

The results from this work, TB90, and NOS93 are summarized in Table IV. When comparing with the previous results, note that the elements in TB90 are referred to the equator of B1950 and have been precessed to J2000 in this work and NOS93.

The mass ratio is the main goal of this work and NOS93, and the values differ by nearly a factor of 2. However, our semimajor axis is consistent with previous results (where the TB90 value is taken from Beletic *et al.* 1989). The elements Ω and u_0 were fixed at the TB90 values in this work. NOS93 describe how they constrained Ω and u_0 to be near the TB90 values. Both this work and NOS93 find a smaller inclination than TB90, although the differences among all three inclinations are larger than the formal errors. This difference is not due to a real change in the inclination, as the observations of NOS93 and this work were taken only 6 months apart. The ~0.25° error in the inclination implies an accuracy of about 0.4%, as does the ~70 km error in the semimajor axis. The apparent orbit of Charon around Pluto is shown in Fig. 5 for all three sets of elements, along with the observed offsets.

5. BOUNDS ON SYSTEMATIC ERRORS

This section investigates possible sources of the difference in the measurement of q by this work and NOS93.

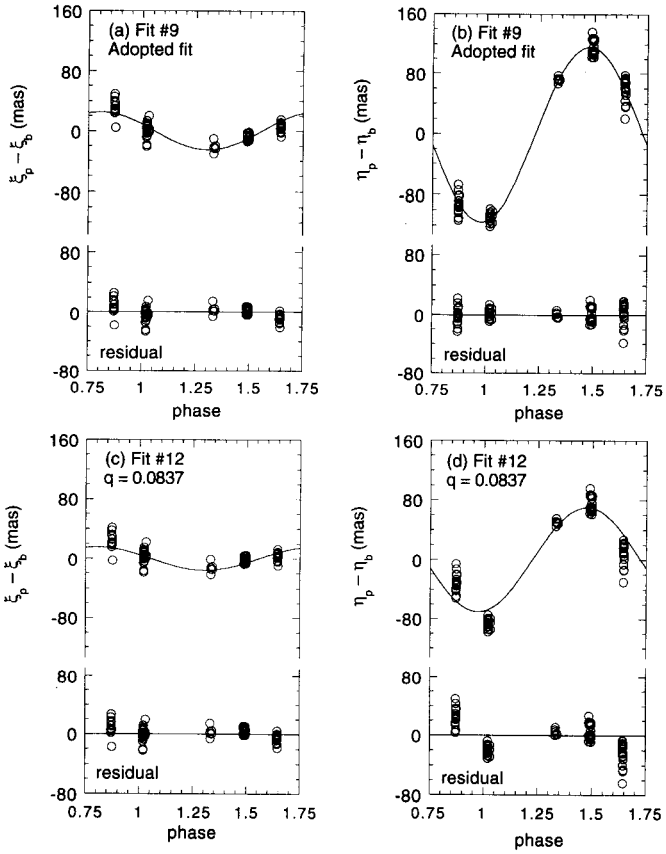

FIG. 4. Pluto's distance from the barycenter in the direction of increasing right ascension ($\xi_p - \xi_b$) and increasing declination ($\eta_p - \eta_b$). Shown are (a) $\xi_p - \xi_b$ for the adopted fit, (b) $\eta_p - \eta_b$ for the same fit, (c) $\xi_p - \xi_b$ for the low-q fit, and (d) $\eta_p - \eta_b$ for the same fit. In the upper portion of each plot, the curve is the model separation and the open circles are the observed separation. The lower portion shows the residuals, at the same vertical scale. Note that the nightly means of the η residuals are clustered around zero for the adopted fit, but are as large as 26 milliarcsec when q is fixed at the value from NOS93.

The effect of random errors on the derived mass ratio should be reflected in its formal error. To the extent they can be modeled, systematic corrections should not degrade the results. Unmodeled or incorrectly modeled systematic corrections can lead to an incorrect measurement of the mass ratio. Table V summarizes the mean random error, the maximum systematic correction, and associated error for the various steps in the analysis.

Both NOS93 and this work found the centers by PSF fitting. The formal errors in the centers were smaller for NOS93 than for this work, because their PSF had a smaller core. Balancing this, we use 80 observations for 5 nights spanning 6 nights, compared with NOS93's 14 observations spanning 4 nights. PSF fitting can introduce systematic errors; if the constructed PSF is a bad match to Pluto at the distance of Charon, Charon's center and brightness are adjusted to compensate. As discussed in Section 4.4

TABLE IV
Bulk Properties for Pluto and Charon

	TB90	NOS93	This Work[a]
Semimajor axis, a (km)	19640 ± 320	19405 ± 86	19460 ± 58
Inclination[b], i (deg)	99.1 ± 1.0	96.56 ± 0.26	95.00 ± 0.24
Long. of ascending node[b], Ω (deg)	223.015 ± 0.028	(223.007 ± 0.041)	(223.015 ± 0.028)[c]
Arg. of latitude[b], u_0 (deg)	259.76 ± 0.08	(260.00 ± 0.24)	(259.76 ± 0.08)[c]
Mass ratio, q	–	0.0837 ± 0.0147	0.1566 ± 0.0035
System mass, M_{sys} (10^{24} g)	14.72 ± 0.72	14.20 ± 0.19	14.32 ± 0.13
Pluto mass, M_p (10^{24} g)	–	13.10 ± 0.24	12.38 ± 0.12
Charon mass, M_c (10^{24} g)	–	1.10 ± 0.18	1.94 ± 0.04
Pluto radius, R_p (km)			
Stellar occultation, clear	1195 ± 5	1195 ± 5	1195 ± 5
Stellar occultation, haze	<1180 ± 5	<1180 ± 5	<1180 ± 5
Mutual events (TB90)	1151 ± 20	1137 ± 8	1140 ± 7
Mutual events (E. Young 1992)	1190 ± 20	1176 ± 7	1179 ± 6
Charon radius, R_c (km)			
Stellar occultation	> 601.5	> 601.5	> 601.5
Mutual events (TB90)	593 ± 16	586 ± 13	588 ± 13
Mutual events (E. Young 1992)	642 ± 11	635 ± 5	636 ± 4
System density, ρ_{sys} (g cm^{-3})			
Stellar-occultation radii , clear	1.81 ± 0.09	1.74 ± 0.04	1.76 ± 0.04
Stellar-occultation radii , haze	> 1.67	> 1.72	> 1.74
Mutual-event radii (TB90)	2.03 ± 0.03	2.03 ± 0.03	2.03 ± 0.03
Mutual-events radii (E. Young 1992)	1.80 ± 0.02	1.80 ± 0.02	1.80 ± 0.02
Pluto density, ρ_p (g cm^{-3})			
Stellar-occultation radius, clear	–	1.83 ± 0.04	1.73 ± 0.03
Stellar-occultation radius, haze	–	>1.82	>1.74
Mutual-event radius (TB90)	–	2.13 ± 0.04	1.99 ± 0.03
Mutual-event radius (E. Young 1992)	–	1.92 ± 0.03	1.80 ± 0.02
Charon density, ρ_c (g cm^{-3})			
Stellar-occultation radius	–	<1.60	<2.22
Mutual-event radius (TB90)	–	1.30 ± 0.23	2.28 ± 0.17
Mutual-event radius (E. Young 1992)	–	1.02 ± 0.17	1.79 ± 0.05

[a] Fit #9.
[b] Referred to the mean equator and equinox of J2000 at epoch JD 2446600.5.
[c] Fixed at value from Tholen and Buie (1990).

of NOS93, their model PSF probably was an inexact match to the actual HST PSF. They established the required systematic correction by fitting the model PSF to synthetic "Pluto–Charon" images constructed from field stars. They found the required systematic correction was up to 10 milliarcsec for Charon, with no significant effect on Pluto. They do not quote an error in the correction, but state that "the larger, well-determined corrections were usually about twice as large as the corresponding solution scatter and were roughly the same for different choices of registration stars. Therefore, an average correction from a combination of several star pairs was selected for Charon centroid calibrations." From this statement we infer that NOS93's error in the systematic correction to fitted centers was roughly 3 milliarcsec.

In this work, fits of the model PSF to synthetic

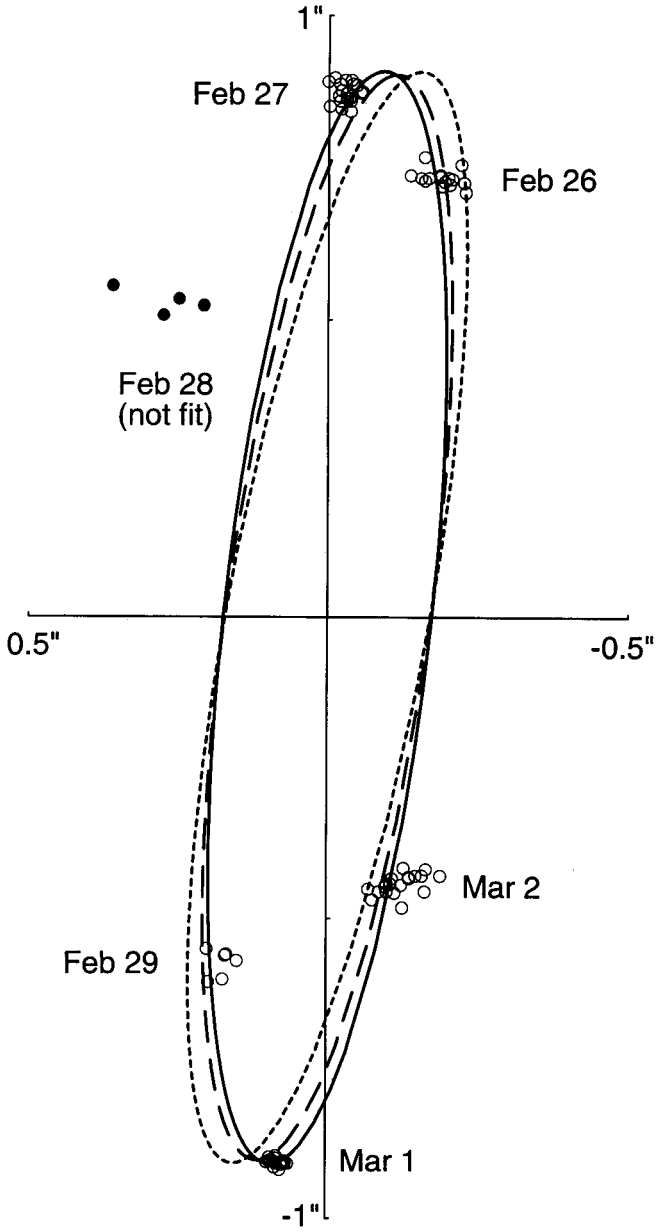

FIG. 5. Charon's orbit around Pluto. The solid line is the adopted solution (Fit #9). The open circles are the observations that were included in the fit. The solid circles were excluded. The dashed line is the orbit from NOS93, and the dotted orbit is for TB90. North is up and east is to the left.

"Pluto–Charon" images implied no systematic correction. Any other result would have been surprising, since the PSF was itself constructed from the field stars. There may still be an unmodeled systematic effect, if Pluto or Charon differed significantly from the mean PSF determined from the stellar images. One such difference is the angular diameter of Pluto, which at 29.4 AU is 0.11 arcsec. For our best images, which have a FWHM of 0.91 arcsec, we can apply the results of Jones *et al.* (1988), who find that Pluto's angular diameter increases the FWHM by 0.5%. The telescope tracked at Pluto rates, during which time the stars' centers move 0.02 arcsec on the detector.

We placed an upper limit on the systematic correction to the center-finding algorithm by fitting Pluto and Charon again, with a different model PSF. The nominal PSF was described in Section 3a. The second PSF was dominated by star 206, and was constructed using backgrounds derived from a sky annulus. We found, as did NOS93, that the Pluto positions were relatively insensitive to changes in the PSF. Pluto centers changed less than 3 milliarcsec. Charon centers changed by 25 milliarcsec for the February 28 data, and by 5–7 milliarcsec for the remaining nights. If the second PSF represented the range of reasonable deviation of PSF's from the nominal, then these changes provided the estimate for the systematic error inherent in the PSF fitting.

The semimajor axes of this work and NOS93 differed by only 0.4% and the inclinations by 1.6°. This agreement was probably not a coincidental cancellation of errors in the image scale and the center-finding algorithms; as evident in Table III, we found the image scale to much better than this accuracy. This implies that the systematic errors in the Pluto–Charon separations are probably less than 0.4% of the semimajor axis, or 4 milliarcsec. The difference in the mass ratio cannot be explained by a difference in Charon's orbit because (i) the two studies find similar orbits, and (ii) both studies find that leaving out the Charon centers increases the formal error, but does not change the mass ratio significantly. Since our tests indicate that Pluto's center is much less sensitive than the separation to changes in the PSF, we believe that the difference in the mass ratio is not due to systematic errors in PSF fitting.

We next consider the effects of stellar aberration, refraction, changes in the tangent point, precession, and nutation on our registration (Section 3b). Precession and nutation are completely removed by defining ξ and η with respect to the equator and equinox of J2000. NOS93 corrected for stellar aberration explicitly, and had no need to correct for refraction. In our work, the registration of exposures implicitly accounted for the linear terms of differential refraction (from the variation in airmass over the field), changes in the tangent point, and aberration. The remaining higher-order terms were less than a milliarcsec. The variation of refractivity with color was important only for star 206, whose position was refracted by about 10 milliarcsec relative to the other stars between the minimum and maximum observed zenith distances. The remaining objects had similar colors, and so their relative positions were not shifted significantly by the variation of refraction with wavelength. In particular, the color of Pluto and Charon over a rotation did not vary

TABLE V
Comparison of Techniques and Sources of Error

	Random Error (milliarcsec)		Systematic Effects (milliarcsec)		Comments	
	This Work	NOS93	This Work	NOS93	This Work	NOS93
Finding centers						
Pluto	±5	±2	0±3	0±0	blended, PSF from field stars	distinct peaks, PSF from literature
Charon	±24	±8	0±7	10±(3)[a]	"	"
Registration	±2	±2	0±1	0±46	6-10 field stars, full linear solution	1 field star, same scale for row & col
Field Distortion	0	0	0±20	89±2	direct imaging	reimaging optics
Center-of-light correction	0	0	4±(4)	10±(10)	Buie *et al.* (1992)	Buie & Tholen (1989)
# of exposures					80	14
Span of data					78% of orbit	50% of orbit

[a] Parenthesized errors are estimated; see text.

enough to significantly change their positions relative to the other stars.

The scatter of the stars' transformed positions provided an estimate of the accuracy of the registration (Section 3b). Figure 6 shows a plot of this scatter (σ_{total}) as a function of the mean of the formal error assigned by Eq. (1) ($\sigma_{\text{Eq. (1)}}$). Assuming Eq. (1) assigned appropriate relative weights, the error introduced by the registration (σ_{reg}) and the ratio of the true errors to the assigned errors (f) was estimated from σ_{total} and $\sigma_{\text{(Eq. 1)}}$:

$$\sigma^2_{\text{total}} = \sigma^2_{\text{reg}} + f^2\sigma^2_{\text{Eq. (1)}}. \quad (8)$$

The best-fit solution (indicated by the curve in Fig. 6) implies $\sigma_{\text{reg}} \approx 2.5$ milliarcsec and $f \approx 1.3$.

The concept of "registration error" had to be modified for the NOS93 observations. In this work, we register the frames to find the positions of Pluto and Charon relative to the field stars. Since there was only one field star present in the NOS93 observations, the equivalent measurement is the angular distance between the field star and Pluto or Charon. The random error introduced was the error in the star's position, 2 milliarcsec. NOS93 assumed that the scale is constant between exposures, and they quoted a stability in the scale of 5 parts in 10^5. Therefore, the systematic errors due to changes in scale with time were less than 0.1 milliarcsec. A more crucial assumption is that the scale in row or line (S_y) equals that in column or pixel (S_x). NOS93 adopted a scale ratio (S_y/S_x) of 1.000 ± 0.002. We evaluated the bounds on the systematic errors implied by the error on the scale ratio; we calculated the Pluto–star separation from Table 4 of NOS93 twice, once assuming $S_y/S_x = 1.000$ and again assuming $S_y/S_x = 1.002$. The second set of separations was multiplied by an overall scale change to minimize the difference between the two sets of separations. The remaining difference is 3–46 milliarcsec, with a mean of 28 milliarcsec. Therefore, the systematic error in NOS93's calculation of the Pluto–star separation is less than 46 milliarcsec. This is a very loose bound on the systematic error, and could account for the difference in the measurements of q. However, NOS93 performed one fit with S_y/S_x as a free parameter, and found that q increased by only 1.1 σ.

NOS93 have up to 89 milliarcsec of field distortion, mainly from the reimaging optics. They determined the field distortion from 5 overlapping exposures of an open cluster. Their maximum error in the field distortion at the locations of Pluto is 2 milliarcsec.

We expected the field distortion for the UH 2.2-m to be insignificant. The back-illuminated CCD is mounted in such a way that it is mechanically supported, which should eliminate the "potato chip" warping that was considered by NOS93 (Gerard Luppino, personal communication). In direct imaging mode, the only optical elements are the primary and secondary mirrors, the filter, and the dewar window. Ray-tracing programs for the 2.2-m optics predicted submilliarcsec field distortions for a range of focus positions (Richard Wainscoat, personal communication).

Although our field distortion is expected to be negligible, we need to place observational limits on this. We have five nights of Midas moving from one corner of the field to the opposite corner, which we used to find an image scale and orientation (Section 4). We use the differ-

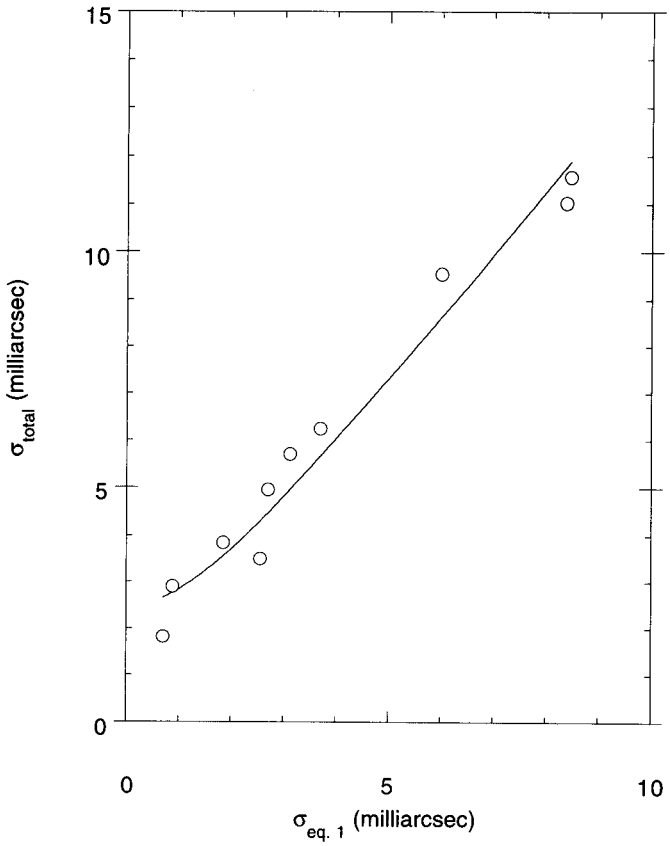

FIG. 6. Residuals in the star positions. For each exposure, a linear transformation of centers was found to minimize the scatter of each stars' transformed position. The scatter is shown as a function of the formal error. The curve is the best fit to $\sigma^2_{total} = \sigma^2_{reg} + f^2\sigma^2_{Eq.(1)}$, demonstrating that the random error introduced by the registration is about 2.5 milliarcsec.

ences between the observed and predicted Midas centers to fit for a field distortion. As the centers follow essentially one path across the field, we can fit for field distortions only along that path. The residual distance (Δd) is the difference between the observed distance (d) and the predicted distance. The residuals were fit with a third order radial function (Eichhorn 1974, Sect. 2.3.7):

$$\Delta d = p_1 d + p_2 d^2 + p_3 d^3. \quad (9)$$

The results of the fit are shown in Fig. 7. There is no apparent field distortion, but we can place only a relatively loose bound of ~20 milliarcsec.

Other assumptions in the model led to small systematic errors. The correction from the observed center of light of Pluto to the desired center of disk depends on the albedo distribution assumed for Pluto. The size of the center-of-light offset is 4 milliarcsec; this serves as a reasonable bound on the uncertainty in position introduced by the model-dependent nature of the albedo maps. Uncertainties in the starting times of the exposures corresponded to errors of 0.01 milliarcsec. Errors in the ephemeris during one week of observation can be simply treated as an offset. The mutual events constrain the eccentricity of Charon's orbit only if the longitude of periapse is not along the line of sight. If it is, the eccentricity could be as high as 0.01, which would introduce a systematic error of 5 milliarcsec.

6. DISCUSSION

The system mass measured by this work and NOS93 are mutually consistent, and represent an improvement over the system mass of Beletic *et al.* (1989). The system density depends on the radii one adopts for Pluto and Charon. If one uses the stellar-occultation radii for a clear atmosphere, the system density is 1.81 ± 0.09 g cm^{-3} and the silicate mass fraction is ~0.6. If one uses TB90's mutual-event radii, the system density is 2.03 ± 0.03 g cm^{-3} and the silicate mass fraction is ~0.7. Triton and Pluto–Charon were probably both formed in the outer solar nebula, about 30–50 AU from the Sun, and therefore probably had the same silicate mass fraction at formation. Triton has a density of 2.07 ± 0.02 g cm^{-3} (Smith *et al.* 1989), for a silicate mass fraction near 0.7. Predictions for the mass fraction at the time of formation range from 0.7 (Anders and Ebihara, 1982) down to 0.5–0.6 (Anders and Grevesse 1989; Grevesse *et al.* 1991). Subsequent to formation, Triton and the Pluto–Charon system had very different dynamical and thermal histories; Triton was captured by Neptune and Pluto–Charon probably experienced a cataclysmic event associated with the formation of Charon. Scenarios for the histories of Triton and the

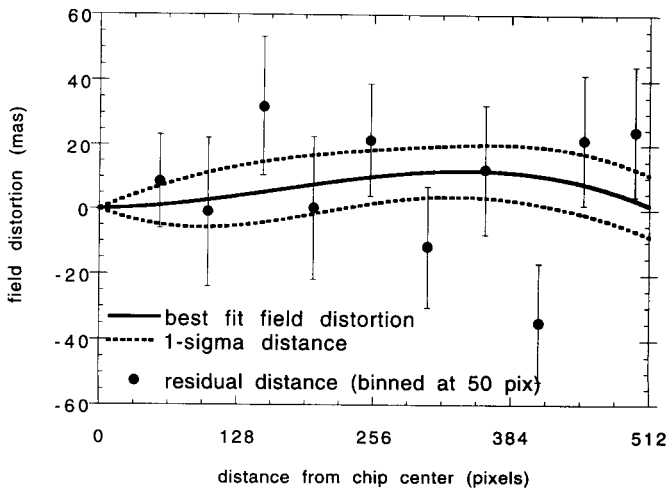

FIG. 7. Field distortion from Midas observations. The 1σ limit of the fit to the field distortion is observed to be less than 20 milliarcsec.

Pluto–Charon system thus appear to fall into one of three broad categories: (i) both were formed with a density near 2.0 g cm^{-3} and neither lost much ice, (ii) both were formed with a density near 1.7 g cm^{-3} and both lost a large fraction of their ice, and (iii) both were formed with a density near 1.7 g cm^{-3} and only Triton lost a large fraction of its ice. We cannot currently distinguish between a high- and a low-density Pluto or Pluto–Charon system. The difference in Pluto's density due to the two observed values of q is small compared with the difference due to the range of reported values of R_p.

The conclusions of NOS93 and this work diverge at this point. We find a mass ratio that is nearly twice as large as that found by NOS93, so our Charon density is nearly twice as large as well. Using Pluto's stellar-occultation radius for a clear atmosphere, we find that Charon is denser than Pluto for $R_c < 644$ km. In contrast, NOS93 find that Charon is much less dense than Pluto for all observed radii. Thus, while the two works indicate similar silicate mass fractions for the system, the distributions are much different. Our Charon mass implies Charon has a silicate mass fraction near that of Pluto (0.5–0.7), while that of NOS93 implies that Charon is mostly ice, with a silicate mass fraction ~0.3.

7. CONCLUSIONS

Contrary to the common wisdom, it is possible to perform precise astrometry of Pluto and Charon from large, ground-based telescopes using PSF-fitting techniques. As Charon's minimum separation increases due to the changing viewing geometry, such measurements will be possible over a greater fraction of the orbit. The challenge in measuring the mass ratio appears to be in calibrating the systematic effects of field distortion and changes in scale and orientation.

We find that the ratio of Charon's mass to Pluto's mass is 0.1566 ± 0.0035. The densities implied depend on the radius of Charon, estimates of which range from 588 ± 16 km (Buie *et al.* 1992) to 636 ± 4 km (Young 1992). In all cases, Charon's density is close to or higher than Pluto's. In sharp contrast, NOS93 find a mass ratio of 0.0837 ± 0.0147, implying that Charon is much less dense than Pluto for all observed radii of Pluto and Charon.

ACKNOWLEDGMENTS

We thank the telescope operators, Bill Mason and Frank Cheigh. Steve McDonald provided the program that generated files from the JPL ephemerides, and the positions of the field stars from both occultation searches. Heidi Hammel gave helpful comments on the manuscript. Portions of this work were supported by NASA Grants NAGW-1991 at Lowell Observatory, and NAGW-1494, NAGW-3296, and AST-8906011 at MIT.

REFERENCES

ACTON, C. H., JR. 1990. The SPICE concept: An approach to providing geometric and other ancillary information needed for interpretation of data returned from space science instruments. In *AIAA/NASA Second International Symposium on Space Information Systems, JPL, Pasadena, CA*, pp. 1029–1052.

ANDERS, E., AND M. EBIHARA 1982. Solar-system abundances of the elements. *Geochim. Cosmochim. Acta* **46,** 2363–2380.

ANDERS, E., AND N. GREVESSE 1989. Abundances of the elements: Meteoritic and solar. *Geochim. Cosmochim. Acta* **53,** 197–214.

BELETIC, J. W., R. M. GOODY, AND D. J. THOLEN 1989. Orbital elements of Charon from speckle interferometry. *Icarus* **79,** 38–46.

BINZEL, R. P., D. J. THOLEN, E. F. TEDESCO, B. J. BURATTI, AND R. M. NELSON 1985. The detection of eclipses in the Pluto–Charon system. *Science* **228,** 1193–1195.

BUIE, M. W., D. J. THOLEN, AND K. HORNE 1992. Albedo maps of Pluto and Charon: Initial mutual event results. *Icarus* **97,** 221–227.

DUNHAM, E. W., S. W. MCDONALD, AND J. L. ELLIOT 1991. Pluto–Charon stellar occultation candidates: 1990–1995. *Astron. J.* **102,** 1464–1484.

EICHHORN, H. 1974. *Astrometry of Star Positions*. Ungar, New York.

ELLIOT, J. L., AND L. A. YOUNG 1991. Limits on the radius and a possible atmosphere of Charon from its 1980 stellar occultation. *Icarus* **89,** 244–254.

ELLIOT, J. L., AND L. A. YOUNG 1992. Analysis of stellar occultation data for planetary atmospheres. I. Model fitting, with application to Pluto. *Astron. J.* **103,** 991–1015.

GREEN, R. M. 1985. *Spherical Astronomy*. Cambridge Univ. Press, Cambridge.

GREVESSE, N., D. L. LAMBERT, AND A. J. SAUVAL 1991. Vibration-rotation bands of CH_4 in the solar infrared spectrum and the solar carbon abundance. *Astron. Astrophys.* **242,** 488–495.

HØG, E., AND J. VON DER HEIDE 1976. Perth 70 catalog. *Abh. Hamburg. Sternw.* **9.**

JONES, J. H., C. A. CHRISTIAN, AND P. WADDELL 1988. Resolved CCD photometry of Pluto and Charon. *Publ. Astron. Soc. Pacific* **100,** 489–495.

KING, I. R. 1983. Accuracy of measurement of star images on a pixel array. *Publ. Astron. Soc. Pacific* **95,** 163–168.

MARSDEN, B. 1989. *Minor Planet Circular,* 14768.

MCKINNON, W. B. 1989. On the origin of the Pluto–Charon binary. *Astrophys. J.* **344,** L41–L44.

MILLIS, R. L., L. H. WASSERMAN, O. G. FRANZ, R. A. NYE, J. L. ELLIOT, E. W. DUNHAM, A. S. BOSH, L. A. YOUNG, S. M. SLIVAN, A. C. GILMORE, P. M. KILMARTIN, W. H. ALLEN, R. D. WATSON, S. W. DIETERS, K. M. HILL, A. B. GILES, G. BLOW, J. PRIESTLEY, W. M. KISSLING, W. S. G. WALKER, B. F. MARINO, D. G. DIX, A. A. PAGE, J. E. ROSS, H. P. AVEY, D. HICKEY, H. D. KENNEDY, K. A. MOTTRAM, G. MOYLAND, T. MURPHY, C. C. DAHN, AND A. R. KLEMOLA 1993. Pluto's radius and atmosphere: Results from the entire 9 June 1988 occultation data set. *Icarus* **105,** 282–297.

MINK, D. J., A. R. KLEMOLA, AND M. W. BUIE 1991. Occultations by Pluto and Charon: 1990–1999. *Astron. J.* **101,** 2255–2261.

NULL, G. W., W. M. OWEN, AND S. P. SYNNOTT 1993. Masses and densities of Pluto and Charon. *Astron. J.* **105,** 2319–2335.

SMITH, B. A., L. A. SODERBLOM, D. BANFIELD, C. BARNET, A. T. BASILEVKSY, R. F. BEEBE, K. BOLLINGER, J. M. BOYCE, A. BRAHIC, G. A. BRIGGS, R. H. BROWN, C. CHYBA, S. A. COLLINS, T. COLVIN,

A. F. Cook II, D. Crisp, S. K. Croft, D. Cruikshank, J. N. Cuzzi, G. E. Danielson, M. E. Davies, E. De Jong, L. Dones, D. Godfrey, J. Goguen, I. Grenier, V. R. Haemmerle, H. Hammel, C. J. Hansen, C. P. Helfenstein, C. Howell, G. E. Hunt, A. P. Ingersoll, T. V. Johnson, J. Kargel, R. Kirk, D. I. Kuehn, S. Limaye, H. Masursky, A. McEwen, D. Morrison, T. Owen, W. Owen, J. B. Pollack, C. C. Porco, K. Rages, P. Rogers, D. Rudy, C. Sagan, J. Schwartz, E. M. Shoemaker, M. Showalter, B. Sicardy, D. Simonelli, J. Spencer, L. A. Sromovsky, C. Stoker, R. G. Strom, V. E. Suomi, S. P. Synott, R. J. Terrile, P. Thomas, W. R. Thompson, A. Verbiscer, and J. Veverka 1989. Voyager 2 at Neptune: Imaging science results. *Science* **246,** 1422–1449.

Standish, E. M. 1987. Jet Propulsion Laboratory Interoffice Memorandum IOM 314.6-891.

Stetson, P. B. 1987. DAOPHOT: A computer program for crowded-field stellar photometry. *Publ. Astron. Soc. Pacific* **99,** 191–222.

Tholen, D. J., and M. W. Buie 1990. Further analysis of the Pluto–Charon mutual event observations—1990. *Bull. Amer. Astron. Soc.* **22,** 1129.

Walker, A. R. 1980. An occultation by Charon. *Mon. Not. Roy. Astron. Soc.* **192,** 47–50.

Young, E. F. 1992. *An Albedo Map and Frost Model of Pluto.* Ph.D. Thesis, Massachusetts Institute of Technology.